



Deposited via The University of Sheffield.

White Rose Research Online URL for this paper:

<https://eprints.whiterose.ac.uk/id/eprint/204181/>

Version: Accepted Version

Book Section:

Altai, Z., Montefiori, E. and Li, X. (2023) Effect of muscle forces on femur during level walking using a virtual population of older women. In: Heifetz, A., (ed.) High Performance Computing for Drug Discovery and Biomedicine. Methods in Molecular Biology, MIMB 2716. Humana New York, NY, pp. 335-349. ISBN: 9781071634486. ISSN: 1064-3745. EISSN: 1940-6029.

https://doi.org/10.1007/978-1-0716-3449-3_15

This version of the chapter has been accepted for publication, after peer review (when applicable) and is subject to Springer Nature's AM terms of use, but is not the Version of Record and does not reflect post-acceptance improvements, or any corrections. The Version of Record is available online at: http://dx.doi.org/10.1007/978-1-0716-3449-3_15

Reuse

Items deposited in White Rose Research Online are protected by copyright, with all rights reserved unless indicated otherwise. They may be downloaded and/or printed for private study, or other acts as permitted by national copyright laws. The publisher or other rights holders may allow further reproduction and re-use of the full text version. This is indicated by the licence information on the White Rose Research Online record for the item.

Takedown

If you consider content in White Rose Research Online to be in breach of UK law, please notify us by emailing eprints@whiterose.ac.uk including the URL of the record and the reason for the withdrawal request.

Effect of muscle forces on femur during level walking using a virtual population of older women

Zainab Altai¹, Erica Montefiori², Xinshan Li^{2}*

¹ School of Sport Rehabilitation and Exercises Sciences, University of Essex, United Kingdom.

² Department of Mechanical Engineering, Insigneo institute for *in silico* medicine, University of Sheffield, United Kingdom.

Author Information

Corresponding Authors

*E-mail: xinshan.li@sheffield.ac.uk, Tel.: +44 (0)1142227786

Keywords: Personalised musculoskeletal model; Muscle volume and force variation; Virtual population; Body-organ coupling; Femoral neck strain; Personal-specific finite element modelling.

Abstract

Ageing is associated with a greater risk of muscle and bone disorders such as sarcopenia and osteoporosis. These conditions substantially affect one's mobility and quality of life. In the past, muscles and bones are often studied separately using generic or scaled information that are not personal-specific, nor are they representative of the large variations seen in the elderly population. Consequently, the mechanical interaction between the aged muscle and bone is not well understood, especially when carrying out daily activities. This study presents a coupling approach across the body and the organ level, using fully personal-specific musculoskeletal and finite element models in order to study femoral loading during level walking. Variations in lower limb muscle volume/force were examined using a virtual population. These muscle forces were then applied to the finite element model of the femur to study the variations in predicted strains. The study shows that effective coupling across two scales can be carried out to study the muscle-bone interaction in elderly women. The generation of a virtual population is a feasible approach to augment anatomical variations based on a small population that could mimic variations seen in a larger cohort. This is a valuable alternative to overcome the limitation or the need to collect dataset from a large population, which is both time and resource consuming.

1 Introduction

Ageing is associated with a combination of both muscle and bone loss. This is particularly relevant in countries such as UK, which faces an increasingly ageing population with rising cost of medical care. In particular, osteoporosis related fragility hip fracture is a major public health issue, which disproportionally affect post-menopausal women due to age and hormonal related bone loss, making bones weaker and more prone to fracture. This is of particular concern with the femur, which is the largest bone of the body and connects to the hip joint to provide mobility.

In the past, the mechanical changes of muscle and load-bearing bone due to ageing were often studied separately owe to limitations in computational power and available data. This limited our ability to understand the mechanical interaction between muscles and load-bearing bones, especially in a large elderly population. Multiple studies have pointed to an association between muscle loss (e.g. sarcopenia) and fall history in epidemiological studies (**1–4**). These results demonstrated the strong mechanical interactions between these two structures in order to enable movements.

The ability to explore intra-personal muscle variations across multiple subjects is important in order to investigate how individual anatomical parameters (such as muscle size, length, path of action) affect kinematics and forces resulting at bones and joints. Previously, anthropometric parameters (e.g., body mass or body mass index) have been used to explain the variation in muscle anatomy. Recent study found large variations in muscle volume, length, physiological cross-sectional area in eleven post-menopausal women between body sides and across the cohort (**5**). However, more than half of these variations remained unexplained. In addition, elderly individuals are known to experience muscle loss at very different rate and extent, which can substantially affect the ability of the muscles to produce force. Muscle strength loss at an older age has been explained by a number of factors, such as a reduction in muscle mass (**6**) and an increase in the percentage of muscular fat with a reduction in

physiological cross-sectional area of the muscle (**6–8**). These factors can be generalised by a general reduction in muscle volume and hence the force produced by the muscle (assuming a linear relationship between muscle volume and muscle force). These variations will affect the estimated isometric force and consequently the loads exerted on femur, hip and knee joints. A series of sensitivity analysis was conducted in order to understand how muscle forces would affect the strain predictions on the femur during level walking in five postmenopausal women (**9**). Results from this initial study indicated substantial differences in the predicted strains across the cases. These findings suggest that intra-personal variations (muscle anatomy/force and bone strength) are substantial and should be further investigated in a larger population.

This study **aims to** investigate how muscle variability (muscle volume and hence muscle forces) affects femoral loading in a large virtual population using the previously developed personalised body-organ coupling procedure (**9**). The variation in muscle forces was estimated at the body level, using a fully subject-specific musculoskeletal model, and data collected during gait analysis. The effect of muscle volume/force variation on the mechanical response of the femoral neck was then investigated using finite element modelling in order to identify the amount of variation in predicted femoral neck strain and any influential muscles during level walking.

2 Methods

This section is split into several parts. First, the participant information and data acquisition details were described. This then leads to the description of personalised musculoskeletal models at the body level and the creation of a virtual population of musculoskeletal models. Maximum isometric muscle forces were extracted from this virtual population to be used as input for the finite element model. The second half of this section describes the generation of a personal-specific finite element model of the femur. The femur's biomechanical responses were simulated and evaluated at two critical time points of the gait cycle through a sensitivity analysis using different muscles forces from the virtual population. This approach provides an elegant coupling between the body and the organ level using individual specific data collected from multiple modalities as well as various engineering techniques across different scales. The general workflow is presented in Figure 1.

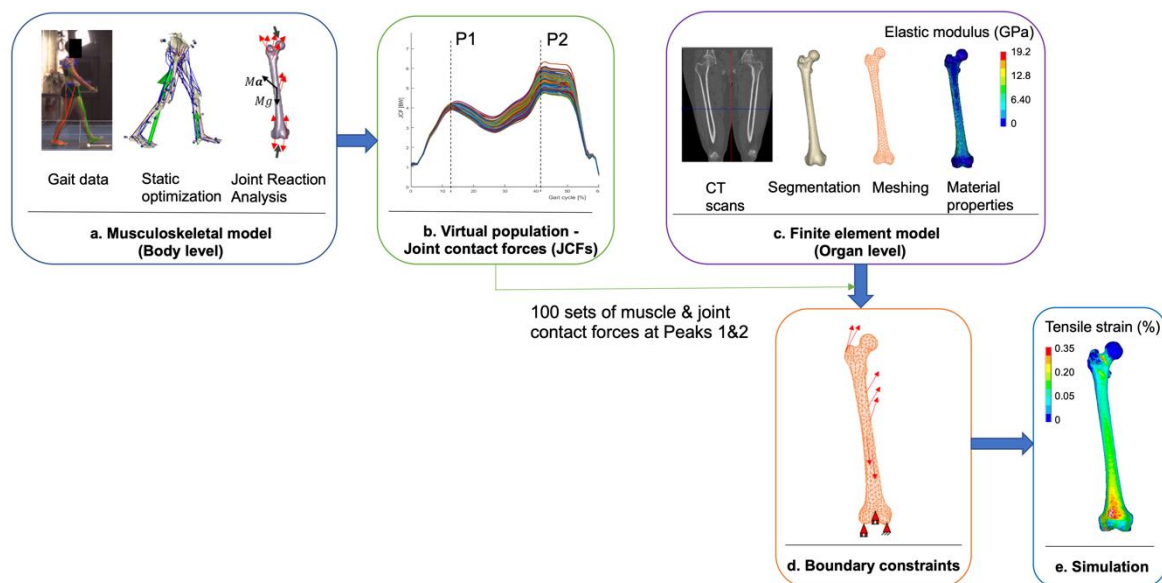


Figure 1. Body-organ coupling pipeline showing the body-level musculoskeletal model (a), the organ-level finite element model of the femur (c), an example joint contact forces of the virtual population (b), the combined model with boundary conditions applied to the femur (d) and a typical simulation result showing tensile strain distribution (e).

2.1 Participants and data acquisition

This study used retrospective data collected as part of an EPSRC funded study (MultiSim and MultiSim2, EP/K03877X/1 and EP/S032940/1), which involved eleven post-menopausal women (69 ± 7 year, 159 ± 3 cm, 66.9 ± 7.7 kg). Inclusion criterion was having a bone mineral density T-score at the lumbar spine or total hip (whichever was the lower value) less than or equal to -1. Those who were obese ($BMI > 35$) or underweight ($BMI < 18$) were excluded. Ethics approval was obtained through the Health Research Authority of East of England (Cambridgeshire and Hertfordshire Research Ethics Committee, reference 16/EE/0049). Each participant was scanned in CT (GE LightSpeed 64 VCT) from the hip to the knee. The CT scan settings were tube current of 120 mA, tube voltage of 100 kVP, and a resolution of $0.742 \times 0.742 \times 0.625$ mm³. Full lower limb MRIs were collected using a Magnetom Avanto 1.5T scanner (Siemens). A T1-weighted sequence was used with a voxel size of $1.1 \times 1.1 \times 5.0$ mm³ for the long bones and $1.1 \times 1.1 \times 3.0$ mm³ for the joints. Each participant was also invited to the gait lab to collect 3D gait analysis data including marker trajectories and ground reaction forces.

2.2 Baseline musculoskeletal models

The 3D gait analysis data and MRI scans of the lower limb were used to build baseline monolateral musculoskeletal models (Figure 1a). These included four body segments (pelvis, femur, tibia, foot) articulated by an ideal ball-and-socket joint for the hip, and two ideal hinges, one for the knee and one for the ankle respectively, as well as 43 lower limb muscles. These 43 lower limb muscles corresponded to the lower-limb muscles included in state-of-the-art OpenSim model gait2392 in the literature (**10**). Out of these, 23 muscles can be reliably segmented and an online repository containing personalised muscle volume and lengths has been created (**5**)¹.

¹ Available from the online repository (<https://doi.org/10.15131/shef.data.9934055.v3>), comprising of all eleven older women enrolled. Note that in this study, for ease of comparison, each of the Adductor magnus, Gluteus maximus and Gluteus medius muscles have been split into 3 bundles.

From these eleven women, one participant (70.5 yr, 61.4 kg, 164 cm, BMI 22.8, T-score of -2.2) was selected to build a fully subject-specific musculoskeletal model (SSMM) and subject-specific finite element model of the femur (described later on). The SSMM was generated using personalised bone geometries and segment inertia generated from MRI (**11**). The joint axes were determined via morphological fitting to the articular surface of the segmented bone geometries. The same set of muscles in gait2392 was included in the SSMM; but their origin, insertion and via points were personalised based on the MRI scans. The personalised muscle information (origin and forces) were later used in the finite element simulation of the femur. Muscle length parameters were linearly scaled from gait2392 values in order to maintain their ratio to musculotendon length. Maximal isometric forces (F_{\max}) of 23 lower limb muscles were personalised using MRI-segmented muscle volume (available from the aforementioned online repository). The F_{\max} of the remaining 14 muscles (not available as they cannot be repeatably measured, e.g. Gluteus minimus, Peroneus longus, etc.) were linearly scaled from gait2392 values based on body mass of the participant.

2.3 Virtual population

One hundred variations of SSMM representing a virtual population of individuals were generated (**12**). First, the mean and standard deviation of 23 muscle forces of the eleven women from the online repository were used to generate normal distributions of F_{\max} , representing a virtual population of older women. Independent random sampling of each muscle force distribution was then carried out in order to create 100 sets of F_{\max} for each of the 23 muscles. These were then used to characterise muscle properties of each variation of the SSMM described in the previous section. A convergence study was carried out in order to determine the number of sampling points to ensure less than 10% error in the normalised overlap of the resulting joint contact force (JCF) curve bands (example shown in Figure1b). This is to remove any anomalies that lead to a JCF pattern outside of the normal range.

2.4 Dynamic simulations and data analysis

Hip, knee, and ankle joint angles, and moments were computed from the baseline SSMMs using the OpenSim 3.3 (**13**) inverse kinematics and inverse dynamics tools relying on MATLAB API (v9.1, R2021b, Mathworks, USA). OpenSim recommended good practice was followed. One hundred runs of static optimisation (where the sum of muscle activations squared was minimised) and joint reaction analysis were carried out in order to estimate the individual muscle (maximum isometric) forces and associated normalised JCFs for each virtual case (Figure 1b). Ideal moment generators (reserve actuators) were included for each degree of freedom in order to provide joint torque when muscle forces could not balance the external moments, although these ideal moment generators were made unfavourable to recruit by assigning them a unitary maximum force.

Maximum isometric muscle forces and resultant JCFs estimated by the SSMMs were extracted at two specific gait time points, corresponding to the first peak (P1) and the second peak (P2) of hip JCFs during one full gait cycle. These forces were then used as loading conditions to simulate the mechanical response of the femur using finite element modelling, as described below.

2.5 Finite element model of the femur

For the one selected patient in Section 2.2, the right full femur was segmented from the CT scans using Mimics 20.0 (Materialise, Belgium). The segmented femur was then automatically meshed with 10-node tetrahedral elements (ICEM CFD 15.0, ANSYS Inc.) using an averaged element size of 3mm (849,069 degrees of freedom), following the mesh convergence study reported in a previous study (**9**) using the same MultiSim cohort. Heterogeneous, elastic isotropic material properties were estimated from the CT attenuation and mapped onto the finite element mesh following a validated material-mapping protocol (Bonemat v3, Rizzoli Institute) (**14–16**) (Figure 1c). The European Spine Phantom was used for bone density calibration. Note that CT scans were required here in order to provide personalised element-based Young's modulus estimation. Such information cannot be obtained through MRI scans.

2.6 Static femoral loading during gait and data analysis

Using the finite element model of the femur generated above, muscle isometric forces estimated from the virtual population (representing 100 virtual elderly women) were applied to the model in order to investigate the effect on predicted femoral strain and mechanical behaviour. In order to apply muscle isometric forces to the femoral model, the orientation of the muscle and joint forces were transformed from the MRI to the CT scans' reference frame using the Iterative Closet Point (ICP) algorithm **(17)**. Eighteen muscle forces were applied to the external surface of the finite element model of the femur as point loads (Figure1d). More details are described in Altai et al. (2021) **(9)**. Each muscle's attachment point was estimated by the SSMM. Forces were then applied to the nearest surface node on the finite element mesh. Relaxed kinematic constraints were applied at the distal end of the femur to prevent rigid body motion and were chosen to replicate the basic movements involved in walking considering the equilibrium of forces estimated by the SSMM. The most distal node of the medial condyle was completely fixed, while only the anterior-posterior and superior-inferior displacements of the most distal node at the lateral condyle was constrained (Figure1d). An extra node in the patella groove was constrained antero-posteriorly **(9, 18, 19)**. Hip and knee joint reaction forces (predicted by the finite element model) were used to verify that the imposed boundary conditions were appropriate and statically equivalent to applying the hip and knee JCFs estimated from the SSMM.

For each virtual subject, peak principal strains (e_1 and e_3) at the femoral neck were predicted at two time points (Peak1 and Peak2) corresponding to the first and second peak of the hip JCF curve. The predicted strains were averaged across the surface nodes using a circle of 3mm radius, to follow the continuum hypothesis avoiding local effects of the load **(20, 21)**. The predicted strains were then compared to the previously published yield strain limit: 0.73% and 1.04% for tensile and compressive strain, respectively **(22)**. The location of the peak strains within the femoral neck region was also analysed. And finally, the peak strain energy density (SED) was computed at Peak1 and Peak2. The femoral neck was chosen as the region of

interest as fracture often occurs here during a sideway fall (**23, 24**). This area is also away from the subtrochanteric region where hip muscles attach to the femur (and hence the locations of applied muscle forces).

The relation between the muscle forces estimated by the SSMM and the femoral neck strains predicted by the finite element models was investigated using Pearson's product-moment correlation. The correlation was considered to be moderate when correlation coefficient (r) is above 0.3 and strong when r is above 0.5, under the hypothesis of a p -value below a significance threshold of 0.05. The statistical analysis was carried out in MATLAB API (v9.1, R2021b, Mathworks, USA).

All simulations were performed on the high-performance computing cluster at the University of Sheffield (ShARC) using ANSYS Mechanical APDL 19.1 (Ansys Inc., PA, USA). For each virtual subject, the computing time used to solve the static finite element model was less than one minute for each selected gait time point.

2.7 Results

Across the 100 virtual subjects, the range of hip joint contact forces (normalised by body weight, BW) predicted by baseline SSMMs (using OpenSim) varied by up to 0.8 of the BW at Peak1 and 3.1 of the BW at Peak2, as shown in Figure 2.

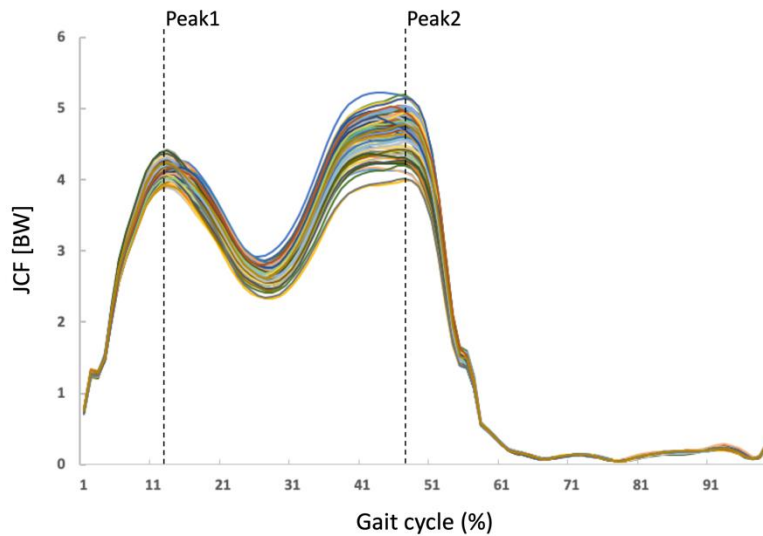


Figure 2. Hip JCFs as predicted by the SSMM for the 100 virtual subjects. The two selected time points of the level walking cycle (Peak1 and Peak2) are indicated by dashed lines.

Using the finite element model of the femur, the principal strains from the 100 virtual subjects were predicted at Peak1 and Peak2 after applying muscles forces. At Peak1, the absolute maximum first and third principal strains (median \pm SD) at the femoral neck were predicted to be 0.37 ± 0.016 % and 0.41 ± 0.016 %, respectively. At Peak2, the absolute maximum first and third principal strains were predicted to be 0.22 ± 0.038 % and 0.27 ± 0.044 %, respectively (Figure 3). There is a wider variation in the predicted principal strains at Peak2 compared to Peak1. The predicted maximum strain energy density (SED, mean \pm SD) at the femoral neck was 4.57 ± 0.46 GPa at Peak1 and 10.73 ± 4.43 GPa at Peak2. The above information is summarised in Table 1.

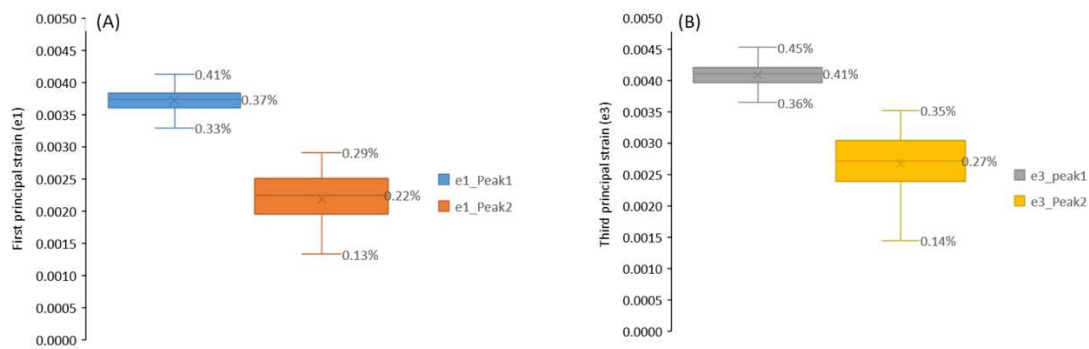


Figure 3. Distribution of the predicted maximum first principal strains (A) and absolute maximum third principal strain (B) at Peak1 and Peak2 of one gait cycle, for 100 virtual subjects.

For all subjects, potential failure (e.g. bone fracture) was predicted to occur under tension. The maximum first principal strains were consistently predicted at the superior-anterior aspect of the femoral neck region in the finite element model for all cases (Figure 4).

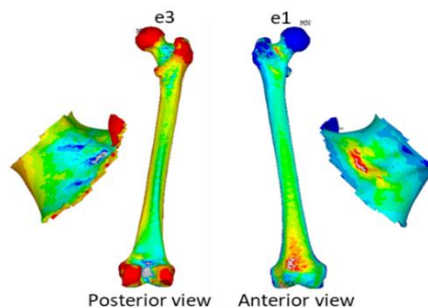


Figure 4. Example distribution of the absolute maximum first (e1) and third principal (e3) strains predicted by the finite element model, shown in anterior and posterior views, with enlarged views for the femoral neck region (i.e. the region of interest).

For most muscles, no statistically significant correlation ($p > 0.05$) was found between muscle volumes (which gave rise to muscle force variations) and the predicted principal strains, as shown in Table 2. However, a few muscles showed significant correlation ($p < 0.05$), which is described here. At Peak1, the Gluteus medius muscle bundles 2 and 3 had a moderate to

strong positive correlation with the principal strains (r in the range of 0.48 to 0.64 for e_1 and e_3 , $p < 0.001$). The Gluteus medius muscle bundle 1 also had a moderate to strong positive correlation ($r = 0.51$ and 0.47 for e_1 and e_3 , respectively, $p < 0.001$) at Peak2. At the second peak, two other muscles showed strong and moderate negative correlation with the principal strains: the Rectus femoris ($r = -0.66$ and -0.68 for e_1 and e_3 , respectively, $p < 0.001$) and the Tensor fasciae latae ($r = -0.44$ and -0.46 for e_1 and e_3 , respectively, $p < 0.001$). For illustration purpose, Figure 5 shows the Gluteus medius muscle volume (bundles 2 and 3) of the 100 virtual subjects plotted against the predicted maximum first principal strains.

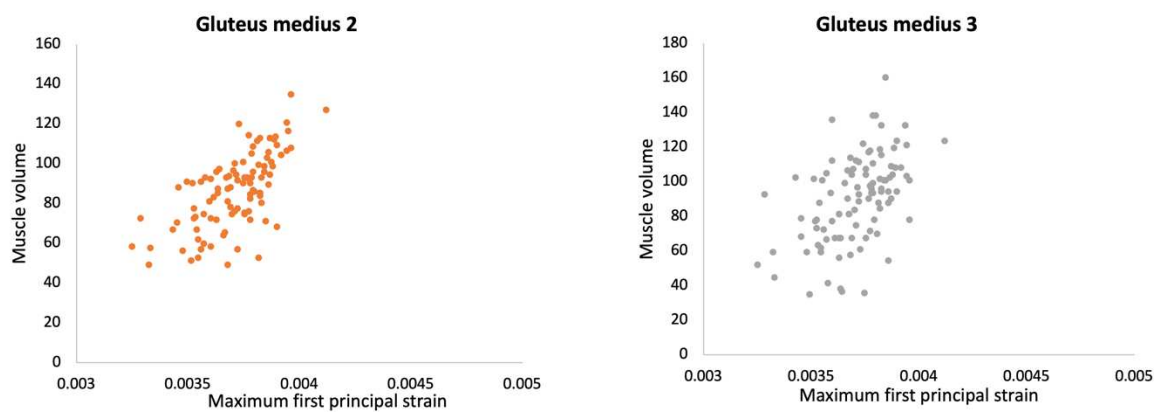


Figure 5. Plot between the Gluteus medius muscle (bundles 2 and 3) volume and maximum first principal strains at Peak1 for 100 virtual subjects.

2.8 Discussion

This study investigated the effects of muscle variability (muscle volume and hence muscle forces) on femoral loading in a virtual population using a personalised body-organ coupling approach. Multibody dynamic models were used to calculate F_{\max} and JCFs, while finite element models of a full femur were used to predict principal strains induced at the femoral neck during one normal walking cycle.

Changes in individual F_{\max} caused variations in the estimated JCFs that were broadly similar to those reported by previous studies, with some small differences (**11, 25, 26**). As previous studies were mainly based on cadaveric values (not live individuals), leading to differences in the definition of the joint axes and muscle paths, and consequently the joint kinematics. In addition, some authors varied all muscle forces simultaneously in the same manner, whereas sampling was carried out in the current study. These differences in approaches could explain the slight differences in results.

The median values of the peak strain (0.22% at Peak1 and 0.37% at Peak2) predicted for the 100 virtual subjects was found to be slightly higher than previous studies (**27, 28**). Kersh et al. (2018) (**27**) reported a median peak strain of less than 0.2% at the femoral neck during walking for twenty subjects, and Martelli et al. (2014) (**29**) reported an average tensile strain of 0.25% at the femoral neck during walking based on a single subject. Both the current study and Kersh et al. (2018) study predicted the maximum strains at the femoral neck region. The difference in predicted strains could be explained by the study design. Kersh et al. (2018) reported values of effective strains, which were calculated from the strain energy density and the Young's modulus of each element across the proximal femur. This is different to the peak principal strains reported here on the surface of the femur. The number of subjects used in this study (100 virtual subjects) was much larger than the previous studies: 20 subjects in Kersh et al. (2018) and 1 subject in Martelli et al. (2014). Furthermore, the current study used fully personalised musculoskeletal and finite element models, while Kersh et al. (2018) scaled the musculoskeletal models from the OpenSim generic model. The MultiSim cohort consisted of elderly women in the osteopenia range (T scores ranged from -2.2 to -1.2), while the subjects in Kersh et al. (2018) ranged between healthy and osteopenia.

Although the predicted strain values were different in these studies, the peak strains in all cases were notably below the fracture threshold (**22**). This finding supports the theory that, in the absence of trauma, bone fracture is only likely to occur when people with weak bones undertake tasks or suffer from accidents that result in high loads.

As shown in Table 2, strong correlations were found between a few muscles and the predicted peak principal strains. For the rest of the muscles, no strong correlation was found between muscle volumes and the strains, with most correlation coefficients ranged between ± 0.2 and 0 (Table 2). The highest positive correlation coefficient ($r = 0.64$, $p < 0.001$) was observed between the Gluteus medius muscles and the first principal strain at Peak1 (Figure5). This is in agreement with previous studies where the Gluteus muscle group was found to contribute to most of the loading on the femur during walking (**9**), as well as when carrying out other tasks such as stair ascent, descent and jumping (**27**). In contrast, the highest negative correlation coefficient was observed for the Rectus femoris muscle ($r = -0.66$, $p < 0.001$ for e1; and $r = -0.68$, $p < 0.001$ for e3) followed by the Tensor fasciae latae ($r = -0.44$, $p < 0.001$ for e1; and $r = -0.46$, $p < 0.001$ for e3) at Peak2. The observed negative correlations suggest that, around the end of the stance phase (toe-off), Rectus femoris and Tensor fasciae latae muscles play a role in lowering the bending strains within the femoral neck by reducing the bending moment on the proximal femur (**30**). A recent study reported similar findings to the current study, where the Gluteus medius muscle was found to be the most influential muscle for more than 40% of the gait cycle, followed by the Rectus femoris (16%), and Tensor fasciae latae (10%) (**31**). As the use of musculoskeletal models coupled with finite element models continues to grow, further investigations are necessary to understand the contribution of each particular muscle on loading the femoral neck during walking.

The highest strains were consistently predicted at the femoral neck region for all virtual subjects. This is likely because the cortical bone at the middle of the femoral neck (current region of interest in this study) is thinner than the rest of the proximal femur. For example, the thicker cortex at the trochanteric region can accommodate higher strains than the femoral neck due to the fact that most hip muscles are inserted around this area. This could have implications in hip fractures due to sideways falls because the thinner cortical bone at the femoral neck cannot bear the substantial bending occurs due to the indirect impact on the greater trochanter.

It is known that muscle forces constitute the largest loads on load-bearing bones (except for case of trauma), which in turn facilitate bone growth, development and remodelling **(32)**. The 'mechanostat' theory states that if the imposed force by muscles exceeds a particular threshold, then bone formation occurs in favour of bone resorption **(32)**. This is reflected by the fact that with smaller Gluteus medius muscle forces, the predicted strains in femur tend to be lower. This indicates that the femur could be more affected by changes in major hip muscles such as the Gluteus medius during ageing. A general reduction in muscle size and power during ageing will lead to a reduction in typical peak voluntary mechanical loading, and consequently remodelling of the bone with reduced bone strength **(32)**. This further illustrates the important mechanical interplay between muscles and load-bearing bones.

The current study has a number of limitations. Only 23 of the 43 muscles included in the lower limb model were personalised in this study. This was due to the lack of repeatability found by Montefiori et al. (2020) **(5)** when segmenting the remaining muscles. Automated algorithms based on machine learning or statistical shape modelling approaches could be developed in future to provide faster and more accurate estimations of muscle volumes. This would enable further studies on the role of the remaining 14 muscles (such as Psoas muscle) that was not included in this study.

In an attempt to preserve subject-specificity in the muscle parameters, physiological cross-sectional area was calculated from muscle volume and length, instead of evaluated directly from higher resolution MRIs **(33)**. Although muscle volume was altered for each muscle in each virtual subject, the specific muscle path remained unchanged. Anatomical variations in muscle path could lead to changes in moment arm. A change in muscle volume and associated force is also expected to cause variations in resulting kinematics, but this was not accounted for in this study. Only the resulting normalised joint contact forces over one gait cycle were checked to ensure the results fell within a reasonable range.

Although a large virtual cohort of 100 subjects were used, this data was based on muscle volume measurements obtained from a small cohort of 11 elderly women with no known

conditions that affected bone or any neurological disorders. This means the virtual population is only representative of elderly women who are relatively healthy in muscle functions. Therefore, the cohort may not be representative of those who suffer from muscle loss associated with sarcopenia or other musculoskeletal diseases.

All finite element models in the current study were created based on a single femur geometry from one selected subject. Information of this same subject was also used to generate the SSMM of all 100 virtual subjects. Therefore, the variation in femur geometry in combination with muscle volume variations was not considered. Collecting fully personalised data for such a large number of subjects is challenging. Future work can include generating such variations in the finite element models using similar approaches as presented here for the musculoskeletal models.

This study focused on only one gait cycle during level walking, although a ten-meter-long walkway was considered during data collection to ensure a natural cadence of the individual while walking, and hence minimising variations. It is known that the gait pattern of an individual may differ in two sequential gait cycles **(34)**, producing different joint, muscle, and ground reaction forces. These changes could induce different strain levels and mechanical responses in the femoral neck. The investigation of the gait variability is beyond the scope of the current study. However, future studies should consider gait variations across different physiological loading conditions and quantify the range of changes in predicted femoral strain.

Acknowledgement All authors received funding from the EPSRC Frontier Engineering Awards, MultiSim and MultiSim2 projects (EP/K03877X/1 and EP/S032940/1). XL has also received funding from the European Commission H2020 programme through the CompBioMed and CompBioMed2 Centres of Excellence and the SANO European Centre for Computational Medicine (Grants N. H2020-EINFRA-2015-1/ 675451, H2020-INFRAEDI-2018-1/823712 and H2020-WIDESPREAD-2018-01/857533).

Table 1. Summary of information predicted at Peak1 and Peak2 of one gait cycle for the 100 virtual subjects. Hip joint contact forces (JCFs) were predicted by the musculoskeletal models. The absolute maximum first (e1) and third (e3) principal strains and strain energy density (SED) were predicted by the finite element models.

Mean \pm SD	Peak1	Peak2
Hip JCFs	0.8 BW	3.1 BW
e1 (median \pm SD)	0.37 \pm 0.016 %	0.22 \pm 0.038 %
e3 (median \pm SD)	0.41 \pm 0.016 %	0.27 \pm 0.044 %
SED (GPa) (mean \pm SD)	4.57 \pm 0.46	10.73 \pm 4.43

BW: Body weight of the selected subject

Table 2. Correlation coefficients (r) between muscle volume (all from the right side) and the predicted absolute maximum first and third principal strains at the two peaks (Peak1 and Peak2) of the gait cycle. Blue; positive correlation. Red; negative correlation. White; no correlation (p -value >0.05).

Muscle	Peak1		Peak2	
	e1	e3	e1	e3
Adductor brevis	-0.03	-0.03	-0.07	-0.08
Adductor longus	-0.05	-0.01	-0.01	-0.01
Adductor magnus 1	-0.17	-0.20	0.08	0.08
Adductor magnus 2	0.08	0.07	0.27	0.27
Adductor magnus 3	0.04	0.05	-0.06	-0.06
Biceps femoris long head	-0.14	-0.16	-0.14	-0.14
Biceps femoris short head	0.20	0.16	0.26	0.26
Gluteus maximus 1	-0.29	-0.26	-0.13	-0.10
Gluteus maximus 2	-0.04	-0.01	-0.09	-0.10
Gluteus maximus 3	0.04	0.08	-0.17	-0.17
Gluteus medius 1	-0.13	-0.24	0.51	0.47
Gluteus medius 2	0.64	0.63	0.04	0.04
Gluteus medius 3	0.48	0.52	-0.03	-0.02
Gracilis	0.03	0.02	0.11	0.10
Iliacus	-0.06	-0.03	-0.10	-0.09
Gastrocnemius lateralis	-0.04	-0.05	0.06	0.05
Gastrocnemius medialis	-0.12	-0.12	0.01	0.00
Peroneus brevis	-0.11	-0.09	-0.05	-0.06
Rectus femoris	-0.23	-0.19	-0.66	-0.68
Sartorius	-0.13	-0.13	-0.02	-0.03
Semimembranosus	0.09	0.05	0.07	0.07
Semitendinosus	0.20	0.19	0.21	0.22
Soleus	-0.18	-0.17	-0.09	-0.07
Tensor fasciae latae	-0.23	-0.21	-0.44	-0.46
Tibialis anterior	-0.08	-0.02	0.08	0.06
Tibialis posterior	0.14	0.11	0.19	0.21

Vastus intermedius	0.11	0.12	0.06	0.08
Vastus lateralis	0.00	-0.03	-0.19	-0.18
Vastus medialis	0.02	0.01	-0.16	-0.14

2.9 References

1. Clynes MA, Edwards MH, Buehring B, et al (2015) Definitions of sarcopenia: associations with previous falls and fracture in a population sample. *Calcif Tissue Int* 97:445–452
2. Woo N, Kim SH (2013) Sarcopenia influences fall-related injuries in community-dwelling older adults. *Geriatr Nurs (Minneap)* 35:279–282
3. Yamada M, Nishiguchi S, Fukutani N, et al (2013) Prevalence of sarcopenia in community-dwelling Japanese older adults. *J Am Med Dir Assoc* 14:911–915
4. Edwards MH, Dennison EM, Aihie Sayer A, et al (2015) Osteoporosis and sarcopenia in older age. *Bone* 80:126–130
5. Montefiori E, Kalkman BM, Henson WH, et al (2020) MRI-based anatomical characterisation of lower-limb muscles in older women. *PLoS One* 15:e0242973
6. Larsson L, Grimby G, Karlsson J (1979) Muscle strength and speed of movement in relation to age and muscle morphology. *J Appl Physiol Respir Environ Exerc Physiol* 46:451–456
7. Rahemi H, Nigam N, Wakeling JM (2015) The effect of intramuscular fat on skeletal muscle mechanics: implications for the elderly and obese. *J R Soc Interface* 12:20150365
8. Yoshiko A, Hioki M, Kanehira N, et al (2017) Three-dimensional comparison of intramuscular fat content between young and old adults. *BMC Med Imaging* 17:1–8
9. Altai Z, Montefiori E, van Veen B, et al (2021) Femoral neck strain prediction during level walking using a combined musculoskeletal and finite element model approach. *PLoS One* 16:e0245121
10. Delp SL, Loan JP, Hoy MG, et al (1990) An interactive graphics-based model of the lower extremity to study orthopaedic surgical procedures. *IEEE Trans Biomed Eng* 37:757–767
11. Modenese L, Montefiori E, Wang A, et al (2018) Investigation of the dependence of joint contact forces on musculotendon parameters using a codified workflow for image-based modelling. *J Biomech* 73:108–118
12. Benemerito I, Griffiths W, Allsopp J, et al (2021) Delivering computationally-intensive digital patient applications to the clinic: An exemplar solution to predict femoral bone strength from CT

- data. *Comput Methods Programs Biomed* 208:106200
13. Delp SL, Anderson FC, Arnold AS, et al (2007) OpenSim: Open-source software to create and analyze dynamic simulations of movement. *IEEE Trans Biomed Eng* 54:1940–1950
 14. Schileo E, Dall'Ara E, Taddei F, et al (2008) An accurate estimation of bone density improves the accuracy of subject-specific finite element models. *J Biomech* 41:2483–2491
 15. Taddei F, Pancanti A, Viceconti M (2004) An improved method for the automatic mapping of computed tomography numbers onto finite element models. *Med Eng Phys* 26:61–69
 16. Morgan EF, Bayraktar HH, Keaveny TM (2003) Trabecular bone modulus-density relationships depend on anatomic site. *J Biomech* 36:897–904
 17. Kjer H, Wilm J (2010) Evaluation of surface registration algorithms for PET motion correction
 18. Polgár K, Gill HS, Viceconti M, et al (2003) Strain distribution within the human femur due to physiological and simplified loading: Finite element analysis using the muscle standardized femur model. *Proc Inst Mech Eng Part H J Eng Med* 217:173–189
 19. O'Rahilly R, Swenson R, Muller F, et al (2008) Chapter 18: Posture and locomotion. In: Dartmouth Medical School (ed) *Basic Human Anatomy*
 20. Qasim M, Farinella G, Zhang J, et al (2016) Patient-specific finite element estimated femur strength as a predictor of the risk of hip fracture: the effect of methodological determinants. *Osteoporos Int* 27:2815–2822
 21. Helgason B, Taddei F, Pálsson H, et al (2008) A modified method for assigning material properties to FE models of bones. *Med Eng Phys* 30:444–453
 22. Bayraktar HH, Morgan EF, Niebur GL, et al (2004) Comparison of the elastic and yield properties of human femoral trabecular and cortical bone tissue. *J Biomech* 37:27–35
 23. Altai Z, Qasim M, Li X, Viceconti M (2019) The effect of boundary and loading conditions on patient classification using finite element predicted risk of fracture. *Clin Biomech* 68:137–143
 24. Verhulp E, van Rietbergen B, Huiskes R (2008) Load distribution in the healthy and osteoporotic human proximal femur during a fall to the side. *Bone* 42:30–35

25. Martelli S, Valente G, Viceconti M, Taddei F (2015) Sensitivity of a subject-specific musculoskeletal model to the uncertainties on the joint axes location. *Comput Methods Biomech Biomed Engin* 18:1555–1563
26. Navacchia A, Myers CA, Rullkoetter PJ, Shelburne KB (2016) Prediction of in vivo knee joint loads using a global probabilistic analysis. *J Biomech Eng* 138:
27. Kersh ME, Martelli S, Zebaze R, et al (2018) Mechanical loading of the femoral neck in human locomotion. *J Bone Miner Res* 33:1999–2006
28. Martelli S, Kersh ME, Schache AG, Pandy MG (2014) Strain energy in the femoral neck during exercise. *J Biomech* 47:1784–1791
29. Martelli S, Pivonka P, Ebeling PR (2014) Femoral shaft strains during daily activities: Implications for atypical femoral fractures. *Clin Biomech* 29:869–876
30. Taylor M, Tanner KE, Freeman MAR, Yettram A (1996) Stress and strain distribution within the intact femur: compression or bending? *Med Eng Phys* 18:122–131
31. Benemerito I, Montefiori E, Marzo A, Mazzà C (2022) Reducing the complexity of musculoskeletal models using gaussian process emulators. *Appl Sci* 12:12932
32. Frost HM (2003) Bone's Mechanostat: A 2003 Update. *Anat Rec - Part A Discov Mol Cell Evol Biol* 275:1081–1101
33. Handsfield GG, Meyer CH, Hart JM, et al (2014) Relationships of 35 lower limb muscles to height and body mass quantified using MRI. *J Biomech* 47:631–638
34. Beauchet O, Annweiler C, Lecordroch Y, et al (2009) Walking speed-related changes in stride time variability: effects of decreased speed. *J Neuroeng Rehabil* 6:32